Instantaneous frequency and wave mode identification in a magnetosheath using few spatial points

Nathaniel E U[a)], Beloff N[b)], and George N J[a)†]

[a)] *Department of Physics, Akwa Ibom State University, Nigeria*
[b)] *University of Sussex, Brighton, UK*

(Received 18 October 2012; revised manuscript received 21 December 2013)

Observational data such as those obtained from the magnetosheath in the downstream of Earth's bow shock have waveforms that differ from those of sinusoidal signals. In practice, they are not even aggregates of sinusoidal signals. Therefore, the frequency decomposition for the data requires technique that will account for the time-varying features of the data that will lead to deduction of physical meaning of the observations. The combination of empirical mode decomposition (EMD) and Hilbert transform has been used for extracting the various contributing oscillatory modes (EMDs) and the instantaneous frequency determination (Hilbert transform) of every physically meaningful mode called intrinsic mode function (IMF). The resulting instantaneous frequencies are used to determine instantaneous wave vectors. The combination of the instantaneous frequencies and wave vectors is useful in the identification of wave modes based on the characteristics of the waves. The results show that EMD-Hilbert can be more reliable than simple Hilbert transform alone.

Keywords: EMD-Hilbert transform, instantaneous frequency and wave vector

PACS: 47.40.−x, 47.35.−i, 47.35.Bb, 47.35.Lf **DOI:** 10.1088/1674-1056/22/8/084701

1. Introduction

The inner magnetosheath close to the bow shock is dominated by Alfven ion cyclotron (AIC) modes, while the middle is characterized by mixed Alfven ion cyclotron and mirror modes.[1] Alfven ion cyclotron waves are left-hand polarized and propagate in the direction parallel to the magnetic field.[2] The data used here for the study of the magnetosheath were taken using Cluster mission instrument for observations made on 18 February 2002 for a period 05:15:30 and 07:35:30 UT. The period is subdivided into six divisions with three zones of twenty (20) minute data, each is chosen for this analysis representing the inner magnetosheath (close to the bow shock), the middle magnetosheath and the outer magnetosheath (close to the magnetopause). The magnetic field profile and its associated intrinsic mode functions, and their instantaneous frequencies for the different chosen regions are computed in both spacecraft and plasma frames. The instantaneous wave vectors, phase velocity, and wavelength in the plasma frame are determined. It is considered to be necessary to measure temperature anisotropy and other anisotropies.[1] Polarization has been used previously for identifying the wave modes.[1,3] It has been analyzed that the dayside magnetosheath displays turbulence at frequencies lower than the local proton frequency.[1]

The analyses of the magnetic field and ion data in the magnetosheath of a quasi-perpendicular bow shock revealed an anti-phase correlation between the magnetic field and the ion data. Frequency decomposition reveals frequency lower than 0.1 Hz.[4] From the analysis which reveals different wave modes in the different regions of the magnetosheath, it becomes obvious that the magnetosheath is non-uniform. This means that the plasma state differs across magnetosheath from the bow shock to the magnetopause. Shevyrev put that the magnetosheath is non-uniform in the transverse (perpendicular) direction. The angle ($\theta_{\rm Bn}$) between the magnetic field and normal determines the mutual orientation of the bow shock and the interplanetary magnetic field (IMF) direction. This, according to Ref. [4], has influence on waves of frequency between 0.02 Hz–1 Hz. It was also mentioned that as angle $\theta_{\rm Bn}$ decreases, the waves across a quasi-parallel shock become highly turbulent, and that this variation is twice that set by a quasi-perpendicular shock. But at frequencies lower than 0.1 Hz,[4] the magnetic field is rather intense in some events for a quasi-perpendicular shock.

Plasma beta β (the ratio of particle pressure to magnetic field pressure) much greater than 1 has been considered to be an instability criterion for mirror mode waves which are identified with compression waves, showing anti-correlation in ion flux density and magnetic field magnitude with linear polarization and zero phase velocity in the plasma frame (see Refs. [1] and [4] and the references therein). It has been shown that the electron flux is steady across the shock from the upstream to downstream, so the choice of ion flux is such that it exhibits high fluctuation in the downstream than in the upstream. In the directions parallel and perpendicular to the average magnetic field direction, the behavior of the amplitudes of variation exhibit a double strength for the parallel component, and this grows to over seven times the strength of magentopause.

†Corresponding author. E-mail: nyaknojimmyg@yahoo.com

© 2013 Chinese Physical Society and IOP Publishing Ltd

This implies that compression waves are dominant according to Ref. [4], which is the properties of both the slow and mirror mode waves. These modes are distinguished by their characteristics. Slow modes waves are identifiable by its non-zero phase velocity in the plasma frame while the mirror modes have zero phase velocities. The mirror mode is characterized with an anti-phase correlation in the magnetic field and density fluctuation. Mirror mode is linearly polarized and is non-propagating wave or standing structure in the plasma frame.

In this report, we use the technique that allows the determination of instantaneous frequencies and wave vectors. Instantaneous frequencies of the different stated zones, the instantaneous wave vectors and the instantaneous phase velocities in the satellite frame are all computed. These computations allow the easy determination of the plasma frame instantaneous phase velocities using Doppler shift equation.[5] These various computed properties of waves reveal the characteristics of waves that enable the identification of the wave modes across the magnetosheath.

1.1. EMD-Hilbert transform

Empirical mode decomposition (EMD)-Hilbert transform is based on the Hilbert–Huang Transform (HHT) which enables the analysis of both nonlinear and non-stationary signals. It can also analyze linear and stationary signals as well.

1.2. EMD

EMD extracts signal from series of mono-components called intrinsic mode functions (IMFs).[6–11] This method is suitable for the analysis of practical and real data having a waveform that is complicated where the application of simple Hilbert results in instantaneous frequency that loses the physical sense of the data. The EMD method is a local and adaptive method of frequency-time analysis, which enables the analyses of stationary and non-stationary signals. Cubic spline line[6] is used to form the envelope through maxima and minima of the extracted signal. Their mean called the envelope mean is considered as the average of the upper and lower lines, and the signal $S(t)$ is given as

$$S(t) = \sum_{i=1}^{n} c_i(t) + r_n, \tag{1}$$

where $c_i =$ IMF, c_1 contains the shortest period component of the signal, and r_n is the residue which is constant.

The extracted intrinsic mode functions (IMFs) have the number of extrema and the number of zero crossings, which are equal or differ at most by one, and the mean value between the upper and the lower envelope equals zero at any point.[5,8] This means that the IMFs are symmetric. One IMF has a unique instantaneous frequency different from the others. Each IMF is a mono-component signal. Hilbert transform is easily applied to each IMF for the determination of instantaneous frequency of each IMF.[3,9–11]

1.3. Simple Hilbert transform (SHT) and instantaneous frequency

Hilbert transform is applied to each IMF component on the assumption that any complicated signal such as real data is composed of many different oscillatory modes, the IMFs. For $C_i(t)$ components, the Hilbert spectrum is given for a real valued signal $S(t)$ as[12–15]

$$H[c_i(t)] = \frac{1}{\pi}\mathrm{PV}\int_{-\infty}^{\infty}\frac{c_i(\tau)}{t-\tau}\,\mathrm{d}\tau, \tag{2}$$

where H is the Hilbert transform operator and PV means the Cauchy principal value of the integral.

Let $H[c_i(t)]$ be $y_i(t)$. $c_i(t)$ and $y_i(t)$ form a complex conjugate pair defining an analytic signal $z_i(t)$ as[16–18]

$$z_i(t) = c_i(t) + \mathrm{j}y_i(t), \tag{3}$$

$$c_i(t) + \mathrm{j}y_i(t) = a_i(t)\,\mathrm{e}^{\mathrm{j}\theta_i(t)}, \tag{4}$$

where $a_i(t)$ is the instantaneous amplitude defined as

$$a_i(t) = [c_i^2(t) + y_i^2(t)]^{1/2}. \tag{5}$$

And θ is the instantaneous phase defined as

$$\theta_i(t) = \tan^{-1}\left[\frac{y_i(t)}{c_i(t)}\right]. \tag{6}$$

Therefore, instantaneous frequency is computed from

$$\omega_i(t) = \frac{\mathrm{d}[\theta_i(t)]}{\mathrm{d}t}. \tag{7}$$

The original signal $S(t)$ can be expressed as

$$S(t) = R\sum_{i=1}^{n} a_i(t)\,\mathrm{e}^{\mathrm{j}\int\omega_i(t)\,\mathrm{d}t}. \tag{8}$$

1.4. Wave vector estimation based on ILW

Unlike the determination of the frequency content which is easily obtained using single or more spacecraft data, the determination of the wave vector requires not less than one spacecraft, and provides the best results for multi-spacecraft data. The estimation of the instantaneous local wave vector (ILW) according to Ref. [13] is demonstrated with measurements along worldliness using real valued measurements of four (4) known space–time trajectories as traced by Cluster II mission electric field instruments. We use ILW and magnetic field data in our analysis to determine the instantaneous wave vector along spacecraft separations, and we use the approach in Ref. [5] to determine the wave vector. The instantaneous wave vector expressed as the spatial gradient of the phase with time is given two fixed probes in Ref. [14]) and multi-probes in Ref. [13] and references therein), the case of multi-probes is given as

$$\boldsymbol{k}_i(\sigma) = -\frac{\Delta_x^{(\alpha,1)}\theta_i^{(\alpha)}(\sigma)}{\Delta_x^{(\alpha,1)}x(\alpha)(\sigma)}. \tag{9}$$

In x, y, and z directions,

$$\boldsymbol{k_i} = \begin{pmatrix} k_x \\ k_y \\ k_z \end{pmatrix}. \tag{10}$$

Using C3 as a reference spacecraft for spacecraft separation vector, x

$$\Delta_x^{(\alpha,1)}\boldsymbol{x}(\boldsymbol{\alpha})(\sigma) := \begin{pmatrix} x^{(1)-(3)} & y^{(1)-(3)} & z^{(1)-(3)} \\ x^{(2)-(3)} & y^{(1)-(3)} & z^{(1)-(3)} \\ x^{(4)-(3)} & y^{(1)-(3)} & z^{(1)-(3)} \end{pmatrix}, \tag{11}$$

$$\Delta_x^{(\alpha,1)}\theta_i^{(\alpha)}(\sigma) := \begin{pmatrix} \theta_i^{(1)-}\theta_i^{(3)} \\ \theta_i^{(2)-}\theta_i^{(3)} \\ \theta_i^{(4)-}\theta_i^{(3)} \end{pmatrix}, \tag{12}$$

where α denotes cluster satellites (C1, C2, C3, and C4), α represents the sample point, i is an integer on the IMF ($i = 1,2,3,\ldots,n$). Balikhin *et al.*[5] have treated the transformation from the projection coordinates which are non-orthogonal to physical coordinates (GSM, GSE, etc.). In this paper, we treat $\hat{A}$ for each sample which gives a 3×3 matrix from the satellite pair separations which are linearly independent. As given in Ref. [5], $\hat{A}$ is also a transformation matrix computed from the magnitude of the satellite pair separation distances to form non-orthogonal basis vectors. Instantaneous wave vector $\boldsymbol{k}$ is computed using the calculated projection of wave vector along satellite separation. $\hat{A}$ is expressed as

$$\hat{A}\boldsymbol{k} = \breve{k}, \tag{13}$$

where

$$\boldsymbol{k} = [\hat{A}]^{-1}\breve{k}, \tag{14}$$

$$\breve{k} = [k_1, k_2, k_3], \tag{15}$$

where 1, 2, and 3 refer to the pairs sat13, sat 23, and sat43. The computed $\boldsymbol{k}$ is the instantaneous wave vector, while $\breve{k}$ is the instantaneous wave vector projection along satellite pair separations. The estimated wave vectors are on the assumption that the minimum wavelength of waves is larger than the minimum separation between spacecrafts. The determination of the instantaneous dispersion relation is based on these computed instantaneous frequencies and wave vectors. The properties of the wave such as the phase velocity and characterisation of waves are deduced from these relations.

2. Observations and results

We choose a period between 05:15–07:35 UT on 18 February 2002 for this study. Figure1 shows the magnetic profile for the field strength collected on 18 Febryary 2002 from 04:00–10:00 UT. We divide the period into six equal subdivisions and choose three periods (Fig. 1) of these subdivisions, viz. 05:15–05:35, 06:15–06:35, and 07:15–07:35 UT. The chosen period was the time when cluster spacecrafts were in the magnetosheath outbound from the magnetosphere towards the Earth's bow shock. The period 05:15–05:35 is marked as zone A chosen close to the magnetopause (outer magnetosheath), the period 06:15–06:35 is marked as zone B chosen in the middle of the magnetosheath (mid magnetosheath), and the period 07:15–07:35 is marked as zone C chosen close to the bow shock (inner magnetosheath). Magnetopause was crossed at about 04:59 UT. The magnetic field data used are averaged over 1 min. The shock regime, when these Cluster spacecrafts traverse the magnetosheath, has an average value for the angle between the magnetic field data and the normal of $\approx 18^\circ$, computed using magnetic coplanarity theorem.[15] This angle indicates a quasi-parallel shock regime. We consider the instantaneous frequencies averaged over one min. We use the average value taken over all the four cluster spacecrafts for the analysis in this report. The plot of instantaneous frequency averaged over four spacecrafts for the period between 05:15:30–05:35:30 UT on 18 February 2002 is shown in Fig. 2.

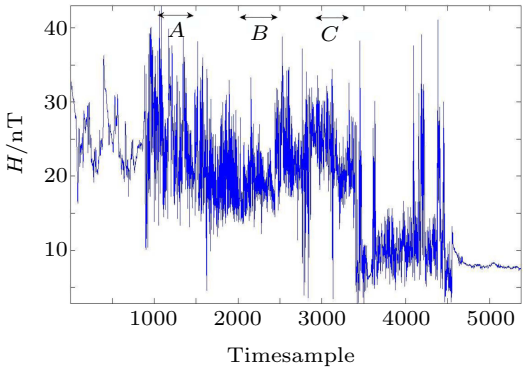


Fig. 1. (color online) Time series plot of magnetic field strength. A, B, and C are the chosen zones for analysis.

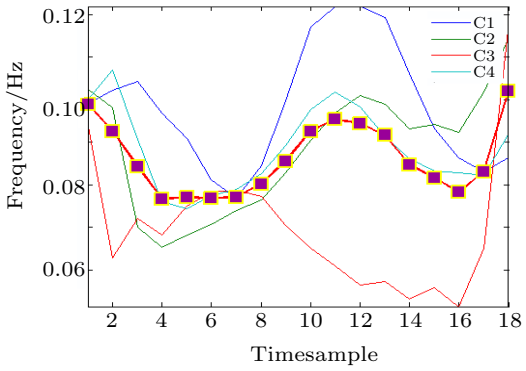


Fig. 2. (color online) Average instantaneous frequencies for four satellites C1, C2, C3, and C4. The line with squares is for the mean taken over all the four spacecrafts whose data are combined with the instantaneous wave vector for the determination of the instantaneous dispersion relations. The data of the y component are considered here. Similar profiles can be plotted for the other time band selected in the magnetosheath for analysis.

Figure 3 shows the computed ratios of the proton perpendicular and parallel temperature. Figure 3(a) exhibits the computed result for zone A, figure 3(b) displays the result for zone

B, and figure 3(c) presents the result for zone C. These are temperature components in the directions perpendicular and parallel to the background magnetic field H. The average value for zone A is 1.079, it is 0.737 for zone B, and it is 1.272 for zone C.

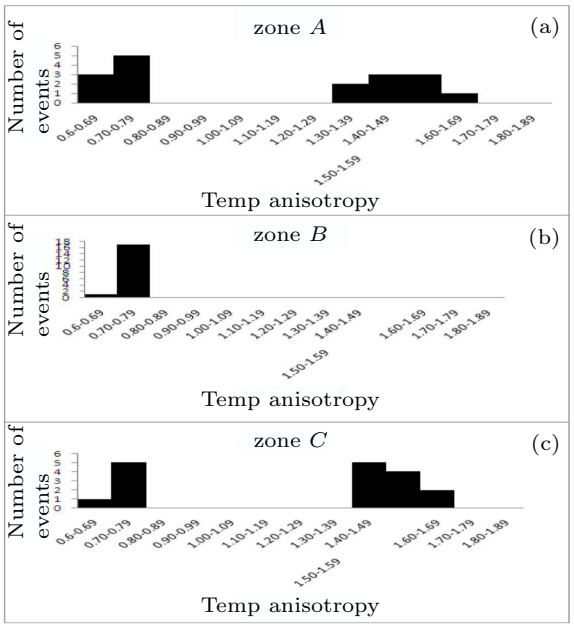


Fig. 3. Histograms of the proton temperature anisotropy in zone A (a), zone B (b), and zone C (c).

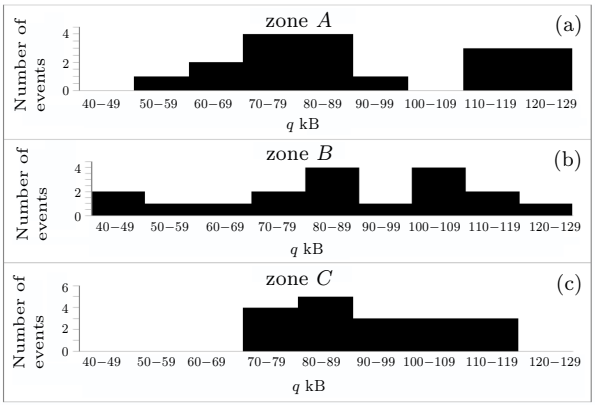


Fig. 4. Angles between the wave vector and magnetic field in zone A (a), zone B (b), and zone C (c).

Figure 4 displays the angles between the wave vector and magnetic field in the three chosen zones. The data for each figure have been averaged over the four cluster spacecrafts. From top to bottom, Fig. 4(a)–4(c) show the histograms for zones A, B, and C respectively. The average value in zone A is about 90°, it is 87° in zone B, and it is 93° in zone C. Figure 5 shows the instantaneous phase velocities in the satellite frame and the plasma bulk velocities. Figure 5(a) shows the satellite frame and plasma bulk velocities computed from data from zone A, Fig. 5(b) displays the satellite frame and bulk velocities computed from zone B, and figure 5(c) exhibits the velocities computed from data from zone C. The average values of the phase velocity and bulk velocity in Fig. 5(a) are $\approx$ 106 km/s and $\approx$ 232 km/s respectively. The average values of the phase velocity and bulk velocity in Fig. 5(b) are $\approx$ 156 km/s and $\approx$ 212 km/s respectively. The average values of the phase velocity and bulk velocity in Fig. 5(c) are $\approx$ 176 km/s and $\approx$ 224 km/s respectively. $V_{\rm ph}$ denotes satellite frame velocity and $V_{\rm pb}$ represents plasma bulk velocity. Figure 6 shows the histograms of the ratio of satellite frame phase velocity to Alfven velocity across the magnetosheath for the selected zones. Figure 7 displays the values of plasma beta β and proton temperatures ratio for the three zones.

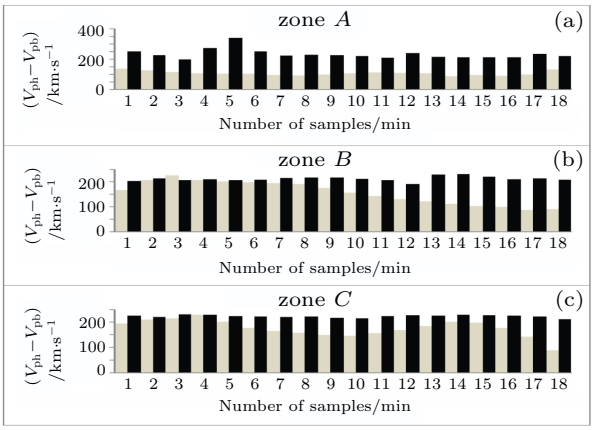


Fig. 5. Instantaneous phase velocities in the satellite frame and the plasma bulk velocities in zones A, B, and C. (a) The average value in the phase velocity is $\approx$ 106 km/s while average value for plasma bulk velocity is $\approx$ 232 km/s. $V_{\rm ph}$ denotes satellite frame velocity and $V_{\rm pb}$ refers to the plasma bulk velocity. Grey represents the phase velocity and black denotes the plasma bulk velocity. (b) The average value in the phase velocity is $\approx$ 156 km/s while plasma bulk velocity is $\approx$ 212 km/s. (c) The average value in the phase velocity is $\approx$ 176 km/s and plasma bulk velocity is $\approx$ 224 km/s.

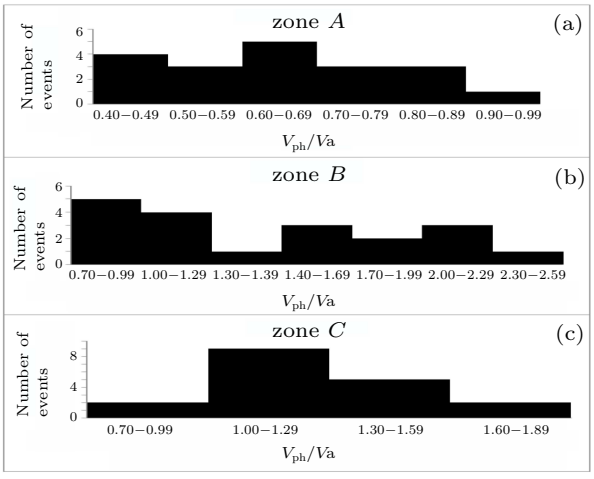


Fig. 6. (a) Histograms of the ratio of satellite frame phase velocities and Alfven velocities across the magnetosheath for selected zones A (a), B (b) and C (c).

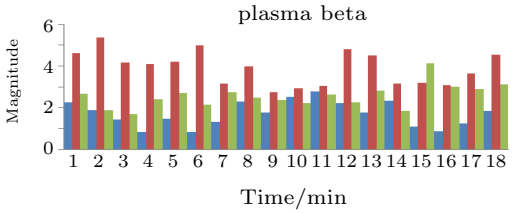


Fig. 7. (color online) Plasma beta β and proton temperature ratios for the three chosen zones *A*, *B*, and *C*. Blue represents zone *A*, red represents zone *B*, and green represents zone *C*.

2.1. Identification of wave mode in the magnetosheath and discussion

Using the parallel and perpendicular proton temperatures observed by CIS instrument of cluster,[19] we compute the temperature anisotropies in the three selected zones to characterize the wave modes using the ratio of $T_{\rm p}(\perp)$ and $T_{\rm p}(\|)$, where $T_{\rm p}(\perp)$ and $T_{\rm p}(\|)$ are the proton temperatures in the directions perpendicular and parallel to the background magnetic field. The results obtained show high plasma beta that vary within the three chosen zones. Comparison of the satellite frame phase velocity with the plasma bulk velocity is carried out which has been used for identifying the wave modes. Computed results of the ratio of the satellite frame phase to Alfven velocity give mean values in a range of 0.60–0.69 for zone *A*, in a range of 1.40–1.69 for zone *B*, and a range of 1.00–1.29 for zone *C*. The relative behaviors of the plasma beta β and proton temperature anisotropies are computed from zones *A*, *B*, and *C*. There is observed the velocity overlap in some parts of the zone. Such characteristics show the existence of a possible mixed mode.

2.2. Wave mode study in the outer magnetosheath (near the magnetopause)

Between 05:15 and 05:35 UT, the wave properties computed using magnetic field, proton, temperature, and velocity data are analyzed. Figure 3(a) shows that zone *A* has a phase velocity lower than the proton cyclotron velocity or Alfven velocity. It also indicates that in the region close to the magnetopause, the waves with phase velocities lower than Alfven proton cyclotron velocity dominates. This lower velocity decreases as the wave approaches to the magnetopause. In this zone there exists a region where the phase velocity normalized to Alfven velocity approaches to unity, towards the middle of the magnetosheath. As earlier mentioned, wave phase velocities lower than the intermediate or Alfven velocities are identified to be of slow mode waves. We can conclude that slow mode waves dominate up to the range of 0:60–0:69 in Fig. 3(a). Also, fluctuations in the satellite frame phase velocity with an average value of 105 km/s exhibit slow mode for plasma bulk velocity of mean value of $\approx$ 232 km/s. Our results show that the value of plasma beta β in this zone is greater than unity but less than those in zones *B* and *C*. Proton temperature anisotropies in zone *A* are close to those in zone *C* but larger than those in zone *B*. Some values of the computed proton temperature anisotropies in zone *A* correspond to those in zone *B* which appear to be constant. We conclude that zone *A* is for a mixture of two modes. Angle between wave vector and magnetic field within this zone varies and has an average value of $\approx 90^\circ$.

2.3. Wave modes study in the middle of magnetosheath

Between 06:15 and 06:19 UT, the estimated instantaneous phase velocities fluctuate in both the satellite frame and in plasma bulk velocity. The average values in both satellite frame and plasma bulk velocities are $\approx$ 210 km/s and 209.5 km/s respectively. According to Ref. [5], the coincidence in the two velocities could only be possible if the wave phase velocity in the plasma frame is zero. According to the above statement, we can confirm mirror mode in this period. Table 1 shows the wave vector interpolated linearly and the angle of the wave propagation direction with respect to the magnetic field between 06:16 and 06:19 UT. Between 06:27 and 06:33 UT, the average value of the computed instantaneous phase velocities in the satellite frame decreases to about 106 km/s with a bulk velocity of $\approx$ 214 km/s. This is close to the computed average value of the Alfven velocity of $\approx$ 110 km/s in this zone. This indicates that this region of the zone is alfvenic. Range of 0.70–0.99 corresponds to the region mentioned in zone *A* (Fig. 6(a)) which is found beyond the range 0.69–0.69. This indicates a mode with phase velocity which is not alfvenic but larger than the slow mode velocity. We conclude that it corresponds to mirror mode wave. The computed instantaneous phase velocity normalized to Alfven velocity gives a range of 1.00–1.29 (Fig. 6(b)), which shows that the computed instantaneous phase velocity is about the value of the Alfven velocity. This indicates that this region is dominated by Alfven wave. Beyond this range, values higher than unity are common. The β is largest in this zone. Angle between the wave vector and magnetic field in this zone varies and has an average value of $\approx 87^\circ$.

Table 1. Wave vectors interpolated linearly and the angles of the wave propagation direction with respect to the magnetic field between 06:16 and 06:19 UT.

k_x/km^{-1}	k_y/km^{-1}	k_z/km^{-1}	$\theta_{\rm kb}$
0.0021	0.0004	0.0011	103.415
0.0022	0.0004	0.0011	97.759
0.0023	0.0004	0.0011	101.748
0.0023	0.0005	0.0012	109.491

2.4. Wave modes study in the inner magnetosheath (near the bow shock)

Between 07:15 and 07:19 UT, the computed phase velocity is higher than the Alfven velocity but close to the plasma

bulk velocity with average values of ≈ 229 km/s for phase velocity in satellite frame and 225 km/s in plasma bulk velocity. The closeness in the values conforms to the earlier case found for a mirror mode in zone *B*. This region corresponds to the region with a range of 0.70–0.99 in histogram of Fig. 6(c), which shares the same behavior with the same range in the histogram of Fig. 6(b). We can conclude that this region in zone *C* is for the mirror mode. Beyond this region between 07:20 and 07:31, the average value for the computed instantaneous phase velocity is ≈ 168 km/s and the average value for the plasma bulk velocity is ≈ 222 km/s. The average value for the computed Alfven velocity is ≈ 167 km/s. This value coincides with the computed satellite frame phase velocity. This confirms that the region of this zone is for Alfven wave mode. The high plasma beta in this zone is lower than that in zone *B*. The temperature anisotropies vary in some places with values corresponding to the uniform values of zone *B*. This indicates that this zone is for a mixture of the characteristics of mirror mode and Alfven mode waves. Angle between the wave vector and magnetic field in this zone varies and has an average value of ≈ 93°.

3. Conclusion

In this article we have used the combination of empirical mode decomposition (EMD) and Hilbert transform known as Hilbert–Huang Transform (HHT) to extract the various contributing oscillatory modes (IMF) and to decompose the frequency of each IMF instantaneously. The resulting instantaneous frequencies are used to determine instantaneous wave vectors. The combination of the instantaneous frequencies and wave vectors is useful for identifying the wave modes based on the characteristics of the waves. The study of the wave modes in the magnetosheath for the three chosen zones *A*, *B*, and *C* has confirmed earlier results which stated the existence of Alfven ion cyclotron, mirror, and slow modes. these modes are related to the activities in the upstream foreshock according to Refs. [3] and [19], and also to the proton temperature anisotropies according to Refs. [1], [2], and [20]. We use satellite frame phase velocity normalized to Alfven velocity in each zone to identify the wave modes. We also use proton temperature anisotropies to support our results. Our results show that zone *A* which is near the magnetopause is characterized with slow mode wave. This zone is also found to have mirror mode, which diminishes towards the magnetopause. We have also found that the ratio of the thermal pressure to the magnetic pressure turns high with thermal pressure in the magnetosheath becoming dominant. This thermal pressure is greatest in the middle magnetosheath found in zone *B*. Mirror mode growth is stable as the proton temperature anisotropy shows larger parallel proton temperature.[21] The mirror instabilities grow when the perpendicular proton temperature is larger than the parallel component.[22] Computed results show that zone *B* is dominantly for mirrror mode. We have also found Alfven ion cyclotron mode in this zone. The inner magnetosheath which is part formed by zone *C* is close to the bow shock, which has been identified with Alfven mode wave based on the computed satellite frame instantaneous phase velocity. Histogram of the phase velocity normalized to Alfven velocity shows peak in a range 1.00–1.29, implying that the wave mode is dominantly Alfvenic. The histogram also shows that this zone is for a mixture of mirror mode and Alfven mode waves.

References

[1] Hubert D 1994 *Adv. Space Res.* **14** 55
[2] Schafer S, Glassmeier K H, Narita, Fornacon K H, Dandouras I and Franz M 2005 *Ann. Geophys.* **23** 3339
[3] Narita Y and Glassmeier K H 2006 *Ann. Geophys.* **24** 2441
[4] Shevyrev N N 2005 *Cosmic Res.* **43** 29
[5] Balikhin M A, Pokhotelov O A, Walker S N and Andre M 2003 *Plan. Space Sci.* **51** 693
[6] Huang N E, Shen Z , Long S R, Wu M C, Shih H H, Zheng Q, Yen N, Tung C C and Liu H H 1998 *Proc. R. Soc. Lond. A* **454** 903
[7] Wu Z and Huang N E 2003 *Proc. R. Soc. Lond. A* **460** 1597
[8] Rilling G and Flandrin P 2006 *On the Influence of Sampling on the Empirical Mode Decomposition* (France: IEEE) p. 4
[9] Huang N E and Shen S S 2005 *Hilbert–Huang Transform and Its Applications* (Singapore: World Scientific) p. 311
[10] Flandrin P, Rilling G and Goncalves P 2004 *IEEE Signal Proc. Lett.* **11** 112
[11] http://www.ens-lyon.fr/~flandrin/software.html
[12] Li H L, Deng X Y and Dai H L 2007 *Mech. Sys. Signal Proc.* **21** 298
[13] Carozzi T D, Buckl A M and Gough M P 2004 *Ann. Geophys.* **22** 2633
[14] Beall J M, Kim Y C and Powers E J 1982 *J. Appl. Phys.* **53** 3933
[15] Paschmann G and Daly P W 2000 *Analysis Methods for Multi-spacecraft Data,* July, 2000, Nether Lands, p. 349
[16] Bedrosian E 1963 *Proc. IEEE* **51** 868
[17] Gabor D 1946 *J. IEEE* **93** 429
[18] Reme H, Aoustin C, Bosqued J M, Dandouras I, Lavraud B, Sauvaud J A, Barthe A, Bouyssou J, Camus Th, Coeur-Joly O, Cros A, Cuvilo J, Ducay F, Garbarowitz Y, Medale J L, Penou A J E, Perrier H, Romefort D, Rouzaud J, Vallat C, Alcayde D, Jacquey C, Mazelle, DUston C, Mobius E, Kistler L M, Crocker K, Granoff M, Mouikis C, Popecki M, Vosbury M, Klecker B, Hovestadt D, Kucharek H, Kuenneth E, Paschmann G G, Scholer M, Sckopke N, Seidenschwang E, Carlson C W, Curtis D W, Ingraham C, Lin R P, McFadden J P, Parks G K, Phan T, Formisano V, Amata E, Bavassano-Cattaneo M B, Baldetti P, Bruno R, Chionchio G, di Lellis A, Marcucci M F, Pallocchia G, Korth A, Daly P W, Graeve B, Rosenbauer H, Vasyliunas V, McCarthy M, Wilber M, Eliasson L, Lundin R, Olsen S, Shelley E G, Fuselier S, Ghielmetti A G, Lennartsson W, Escoubet C P, Balsiger H, Friedel R, Cao J B, Kovrazhkin R A, Papamastorakis I, Pellat R, Scudder J and Sonnerup B 2001 *Ann. Geophys.* **19** 1303
[19] Constantinescu O D, Glassmeier K H, Decreau P M E, Franz M and Fornacon K M 2007 *Ann. Geophys.* **25** 2217
[20] Denton R E 2000 *Int. J. Geomagn.* **2** 1
[21] Lu Q M and Wang S 2005 *Chin. J. Astron. Astro-Phys.* **5** 192
[22] Gray S P 1992 *J. Geophys. Res.* **97** 8519